JOURNAL OF MATERIALS SCIENCE **37** (2002) 3307–3313

Pre-holed tensile specimens for superplastic Y-TZP ceramics

K. SASAKI*, M. NAKANO, Y. IKUHARA, T. SAKUMA
Department of Materials Science, Faculty of Engineering, The University of Tokyo, Tokyo 113, Japan

A new method was developed to produce tensile specimens with pre-machined holes for superplastic zirconia ceramics. Tensile specimens with effective hole sizes of 450 μm were successfully produced using graphite fibers. Although the size of the defect introduced is relatively large compared to the grain size enough deformation is obtained for qualitative and quantitative analysis for Y-TZP. 3Y-TZP and 3Y-TZP co-doped with germanium and titanium oxide revealed cavity growth coefficients that varied with strain rate and temperature, unlike metals, as a direct consequence of grain growth induced strain hardening.

1. Introduction

The evolution of cavities during deformation is a major concern for the mechanical reliability of superplasticaly formed ceramic components. During high temperature deformation failure of the tensile specimens occurs by nucleation, growth and interlinkage of cavities. In metals it is now generally accepted that the growth of cavities mainly occurs by plastic flow, as evidenced by the considerable experimental and theoretical attention in the literature [1–10]. In ceramics, most investigations have been undertaken on the characteristics of cavity evolution in superplastic zirconia ceramics [11–19]. This has been carried out by the observation of the actual cavities during tensile elongation or by the insertion of air bubbles [16] during the processing of the zirconia specimens. Microstructural inspection of deformed zirconia specimens indicated that cavities nucleated predominantly at triple grain boundary points. The level of cavitation in a specimen increased with proximity to the fracture tip, where extensive cavity coalescence could be observed perpendicular to the tensile axis.

Tensile specimens with pre-machined holes have been reported in superplastic metals [20–22]. This kind of approach has the advantage of allowing the observation of one circular defect, avoiding the statistical problems associated with averaging data collected from a wide range of cavity sizes. In the latter stages of deformation, cavity coalescence occurs, but is difficult to quantify this, as can be seen from Fig. 1 for a 500% deformed GeO_2-TiO_2 co-doped 3Y-TZP; therefore, it is preferred to follow the growth characteristics of one particular defect.

Unlike metals it is very difficult to machine very small holes into the gage of tensile specimens. This is due to the inherently brittle nature of ceramics and the fact that 500 μm drills that can successfully penetrate zirconia are firstly expensive and have rarely been produced successfully. In this paper a relatively new and successful method of producing 500 μm holes along the gage length of the tensile specimens will be reported. The change in hole morphology will be investigated for two extreme superplastic materials, a standard yttria stabilized tetragonal zirconia polycrystals (TZP) and a GeO_2-ZrO_2 doped TZP which has shown elongations as large as 1000% [23].

2. Experimental procedure

Commercially available 3 mol% yttria stabilized zirconia high purity powder (Tosoh Co. Ltd.) was used. Co-doped Y-TZP was also employed using germanium oxide (Rare Metallics, 6N) and titanium oxide (Sumitomo Osaka Cement Co. Ltd., 3N) for a composition of 2 mol% Ge-2 mol% Ti (2Ge-2Ti) added to a 3Y-TZP. The co-doped zirconia was prepared by ball milling the starting powders, using zirconia balls for 24 hours in ethanol in polyurethane pots. The co-doped zirconia powder was then dried under an argon atmosphere and granulated with a 25 μm sieve.

In order to obtain holes in the as sintered state, graphite fibers 0.5 mm in diameter (Pentel Co., Japan) were placed in the middle of the die parallel to the compression axis prior to pressing in the die. The powders were pressed into bars at 33 MPa, and then cold isostatically pressed at 100 MPa in a rubber tube. Upon sintering at 1400°C in air for 2 hours, the graphite fibre would burn leaving a circular hole in the sintered body as shown in Fig. 2. Machining of the specimen was carefully undertaken such that the hole would be present in the middle of the gage of 2.2×2.2 mm^2 and a gage length of 13.4 mm. The tensile tests (SHIMAZU AG-5000C) were carried out at 1400–1500°C at constant cross head speeds. Optical microscopy (Nikon,

Present Address: General Electric International Inc., Tokyo, Japan.

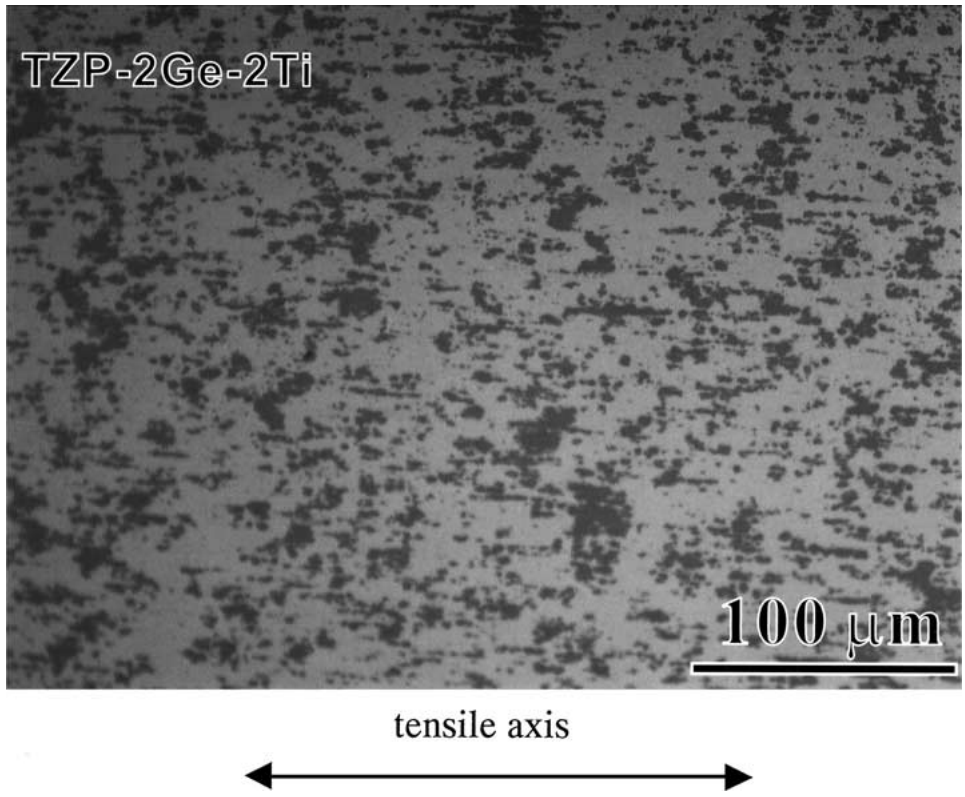

Figure 1 Optical micrograph of failed 2Ge-2Ti at 1400°C, initial strain rate of 1.4×10^{-4} s^{-1}.

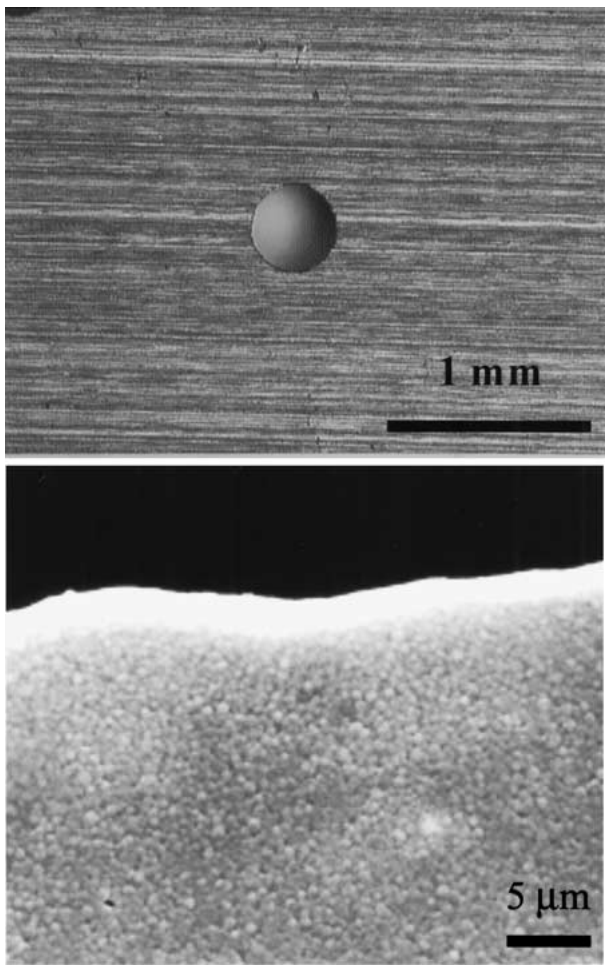

Figure 2 Optical micrograph of tensile specimen using 0.5 mm graphite fiber (top) reduced to 0.45, SEM micrograph of hole edge (middle) and SEM micrograph in the interior of the tensile specimen.

Japan) was used to determine the change in shape of the holes after deformation. The best fit for the size of the holes was obtained by image analysis software. SEM analysis (JEOL JSM-5200) was undertaken for microstructural investigations.

3. Results

Tensile specimens with circular holes using graphite fibres having a diameter of 500 μm were successfully produced and can be seen in Fig. 2. The use of graphite fibres to produce the holes was crucial for this process due to the compatibility between the coefficient of thermal expansion of the fibre and the shrinkage rate of the green body, avoiding the formation of cracks during sintering. Furthermore the relatively low temperature oxidation has allowed the successful removal of the graphite, as carbon dioxide, during sintering. Notice that the final size of the holes is smaller than the initial graphite material used. This is caused by the reduction in volume during sintering of the green bodies. SEM analysis was used to confirm the microstructural uniformity throughout the as-sintered specimen shown in Fig. 2. It was found that the grain size near the hole and the bulk of the specimen were found to have the same values ($\sim$0.45 μm).

The micrographs of the deformed samples taken at 1400°C (with an initial strain rate of 1.4×10^{-4} s^{-1}) are shown in Figs 3 and 4. It can be seen that in both cases the deformed samples have clear elliptical deformation along the tensile axis. The 3Y-TZP specimen failed at around 30% strain whereas the 2Ge-2Ti specimen failed at around 110%. The introduction of the circular defects reduced the tensile properties of both

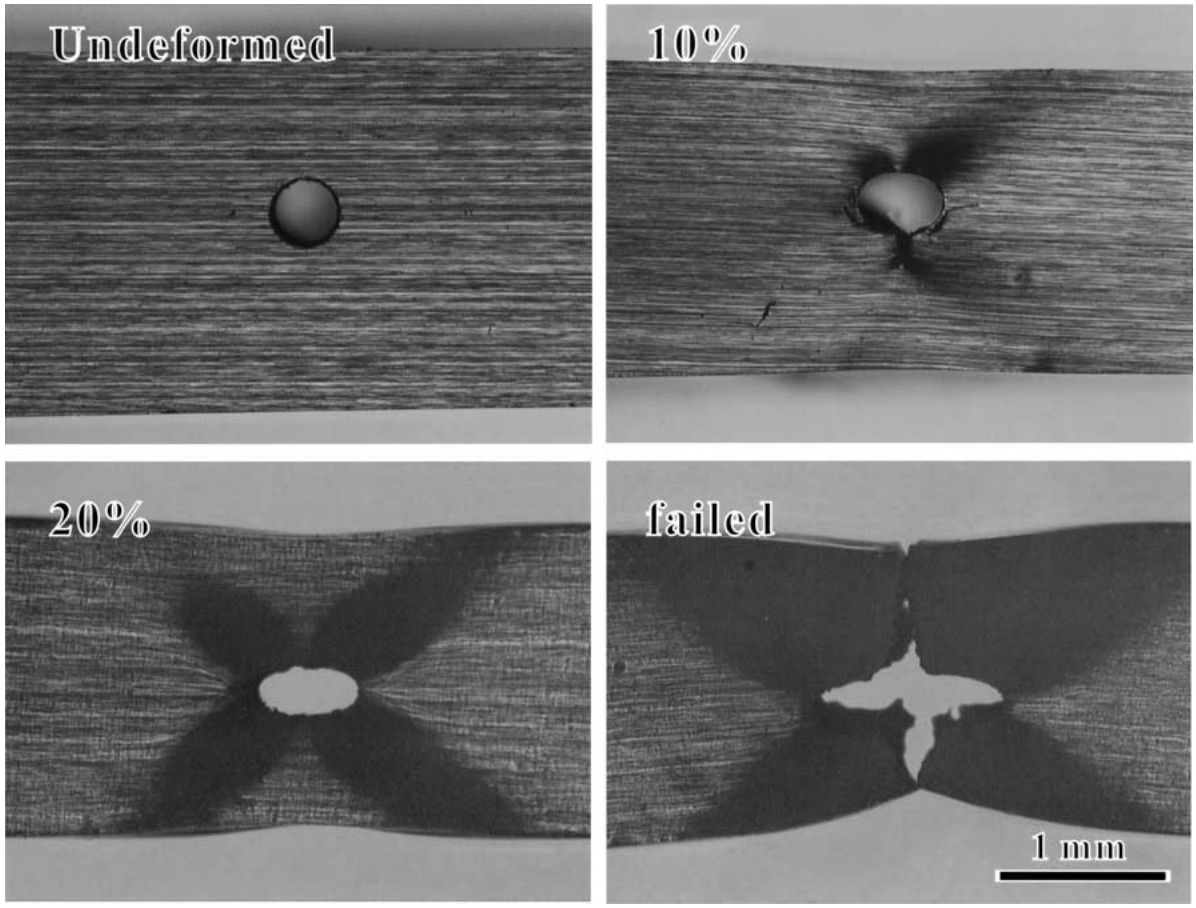

Figure 3 3Y-TZP deformed to various strains at 1400°C, initial strain rate of 1.4×10^{-5} s^{-1}.

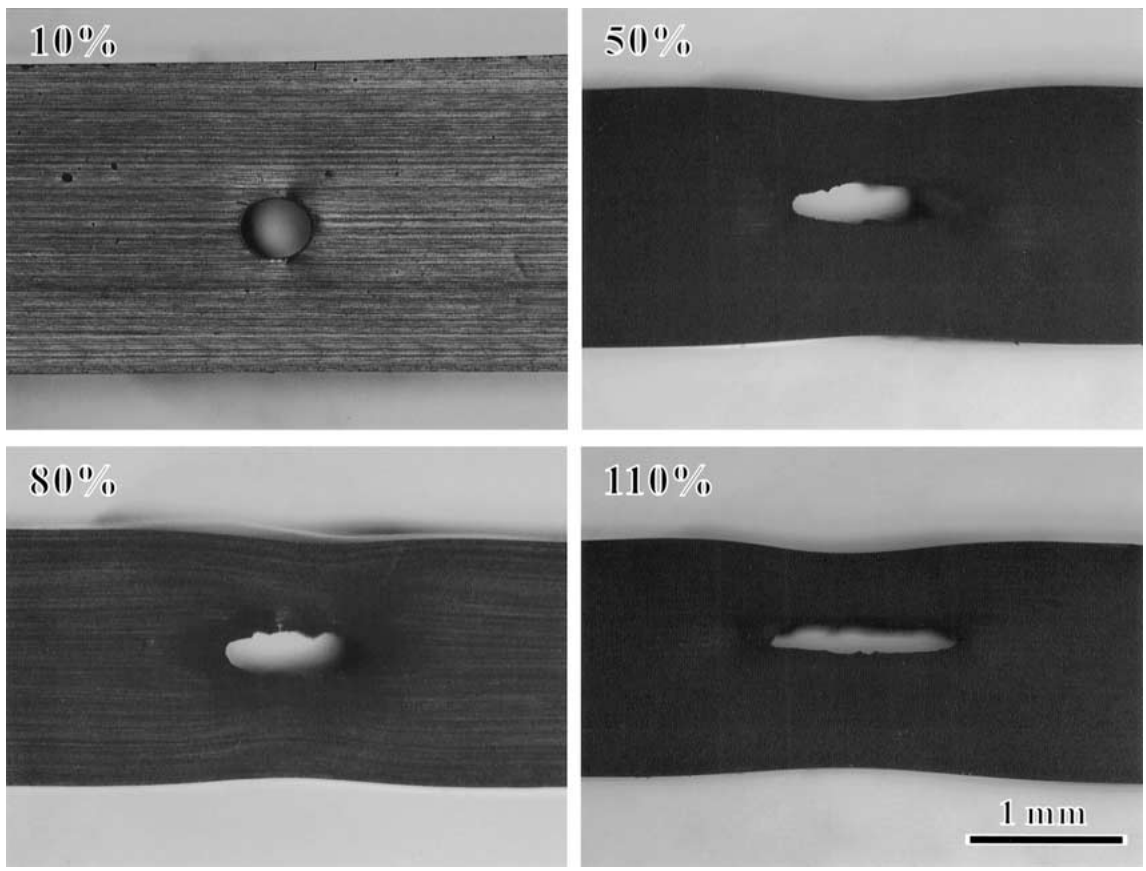

Figure 4 2Ge-2Ti deformed to various strain at 1400°C, initial strain rate of 1.4×10^{-5} s^{-1}.

materials considerably (cf. 130% of 3Y-TZP and 988% of 2Ge-2Ti).

Another interesting feature observed in the deformed specimens is the appearance of shadowed areas emanating at 45° to the tensile axis from the hole, resulting in necking around the hole (Figs 3 and 4) caused by the stress state during deformation. Typically in cylindrical tensile specimens, symmetry around the tensile axis is isotropic. When a tensile specimen with a rectangular cross section with a width that is greater than the thickness is deformed two types of tensile flow instability occur. The first is diffuse necking, which is analogous to the necking found in cylindrical tensile specimens, which arises from the basic tensile instability criterion proposed by Considère [24].

The other deformation process that occurs and often follows diffuse necking is called localized necking. In this mode the neck region is a narrow band with a width equal to the sheet thickness inclined at an angle to the tensile axis, across the width of the specimen. In localized necking there is no change in the width measured along the trough of the localized neck, such that it corresponds to a state of plane-strain deformation. Similarly the bands observed in the current study correspond to localized necking as a consequence of the geometrical constrictions imposed by the presence of the hole.

Investigation of the "fracture tip", revealed another interesting feature of the two samples. The micrographs of the failed specimens are shown in Fig. 5. In the 3Y-TZP cavity formation has only occurred in the volume surrounding the hole. The cavities in these regions have formed limited stringers with crack like cavities extending perpendicular to the tensile axis. The fracture edge of the 3Y-TZP sample is jagged indicating

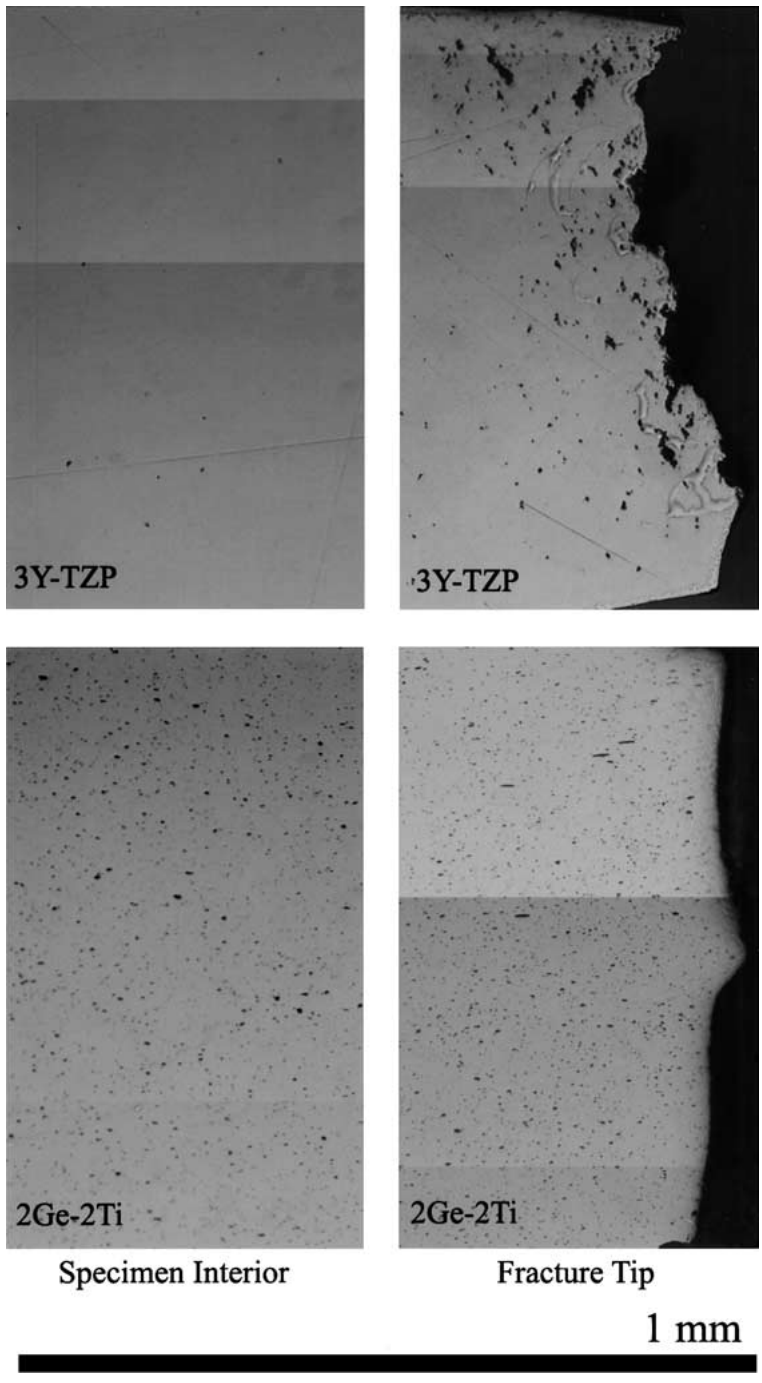

Figure 5 Optical micrographs of 3Y-TZP and 2Ge-2Ti taken at fracture tip and specimen interior tested at 1400°C and 1.4×10^{-4} s^{-1}.

that failure has occurred by the interlinkage of cavities. 2Ge-2Ti shows extensive cavity formation both in the bulk and around the circular hole. The cavities have formed independently with no interlinkage growing parallel to the tensile axis and no crack like cavities growing perpendicular to the tensile axis (Fig. 5). The fracture edge, unlike 3Y-TZP, has occurred in a very clean manner, most likely by simple grain boundary fracture.

To analyze the deformation characteristics of the holes, several geometrical and bulk values can be obtained. The holes were measured using r_1 and r_2 which are the major and minor radii of an ellipse. The average hole radius, r was estimated from the expression:

$$r = \frac{(r_1 + r_2)}{4} \tag{1}$$

while the area, A_h, of an ellipse is obtained as:

$$A_h = \frac{\pi r_1 r_2}{4} \tag{2}$$

The measured dimensions of the holes in the two types of samples were then plotted with respect to strain. Care was taken in the definition of the strain and two forms of strain were employed. The first is the far field strain, ε_{ff} and is defined as:

$$\varepsilon_{\text{ff}} = \ln\left(\frac{A_0}{A}\right) \tag{3}$$

where A and A_0 are the current and initial cross sectional areas of the sample but remote from the holes. The second is the local strain ε_l, which is determined as in the far-field case, but using the dimensions around the cross sectional area of the hole prior to and after deformation. The local strain gives a measure of the degree of local necking and the influence of hole growth on necking.

Fig. 6 shows the normalized change in dimension of the holes in terms of their major and minor axis for several initial strain rates plotted as a function of local strain. Growth primarily occurs in the direction parallel to the tensile axis, while contraction of the void occurs clearly lateral to the tensile axis.

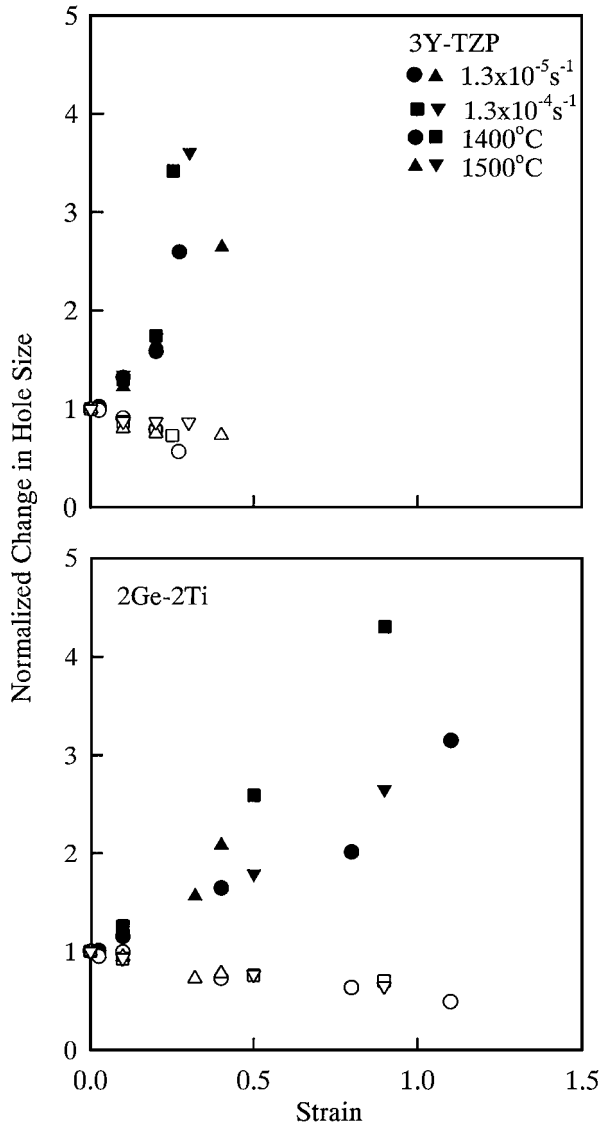

Figure 6 Normalized hole radii with respect to total strain for 3Y-TZP and 2Ge-2Ti (filled symbols parallel to tensile direction and open symbols are perpendicular to tensile direction).

4. Discussion

Using these pre-holed tensile specimens it was possible to obtain additional information on the stress concentration characteristics of these two materials. This was observed from the fracture characteristics of Fig. 5, where it was found that at these testing conditions, stress concentration around a macroscopic defect are very high in the case of 3Y-TZP. 2Ge-2Ti on the other hand indicates a superplastic material having a very high resistance towards stress concentrations. This results in the homogeneous nucleation and growth through out the material of "secondary cavities".

Sufficient data was also collected to analyse the growth characteristics of cavities by plastic flow, which has received considerable theoretical attention in the literature. Using the experimental variables many reports have presented empirical and theoretical models to predict the growth of cavities during superplastic deformation. They all predict that under uniaxial flow a void grows according to:

$$\frac{dr}{d\varepsilon} = kr \tag{4}$$

where k is the void growth parameter and depends on the shape of the void as it grows. Different assumptions made for the various models predict different values of k. The theoretical work of Cocks and Ashby [5] has often been adopted to characterize the growth of cavities. More recently Wang *et al.* [16] have investigated the cavity growth characteristics in TZP where the following expression was employed for the theoretical value of k:

$$k = \left(\frac{1+m}{2m}\right)\sinh\left(\frac{2\rho}{3}\frac{2-m}{2+m}\right) \tag{5}$$

where m is the strain rate sensitivity for a material where deformation is totally attributed to (i) no grain boundary sliding occurs ($\rho = 1$) and (ii) to that where only grain boundary sliding ($\rho = 2$) occurs. The void growth coefficient for cavities is thus dependent on the strain rate sensitivity and is predicted not to change with strain

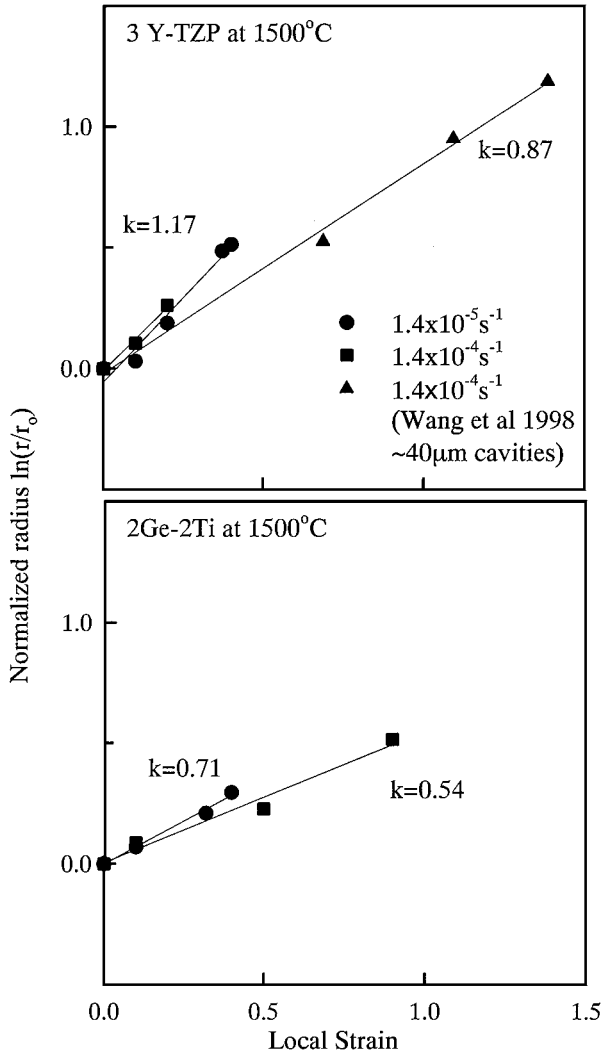

Figure 7 Verification of cavity growth coefficient using Equation 4.

rate. The data obtained in the current study was plotted as a function of void area against the local strain shown in Fig. 7. For 3Y-TZP the values obtained by Wang *et al*. [16] are also shown. The void growth behavior of 3Y-TZP is not far off from the experimental data obtained by Wang *et al*. and there are mild differences with respect to strain rate. However 2Ge-2Ti shows a smaller cavity growth behavior and a corresponding smaller k value.

Table I shows the values obtained from the experimental data and those predicted by Equation 4 using the strain rate sensitivities obtained previously. Although the values for 3Y-TZP lie within the predicted values both in terms of temperature and strain rate, they are closer to a rigid grain mechanism. This is not in accordance with the experimentally observed and generally accepted fact that superplasticity in zirconia occurs by grain boundary sliding. Further the values obtained for 2Ge-2Ti differ quite notably showing differences in k with respect to the theoretical predictions.

TABLE I Experimental and calculated grain growth coefficients obtained at 1500°C

Sample	ε (S^{-1})	m	k, experimental	k, calculated
3Y-TZP	1.4×10^{-4}	0.26	1.28	1.28–1.91
3Y-TZP	1.4×10^{-5}	0.26	1.17	1.28–1.91
3Y-TZP [16]	1.0×10^{-4}	0.5	0.87	0.56–1.33
2Ge-2Ti	1.4×10^{-4}	0.39	0.54	0.85–1.88
2Ge-2Ti	1.4×10^{-5}	0.39	0.77	0.85–1.88

The expression used by Wang *et al*. predicts that cavity growth will be restricted with increasing strain rate sensitivity as can be seen from the experimental results of 3Y-TZP and 2Ge-2Ti. However Equation 5 does not predict any changes in k with respect to strain rate (or testing temperature). The discrepancy in the values of k is due to the fact that the expression for k originates from power law creep and thus predicts the growth of holes mainly on the strain rate sensitivity. However during deformation strain hardening induced by grain growth also occurs and may be the cause of such discrepancies.

Unlike the previous pre-holed tensile specimens of superplastic metals, no major macroscopic cavity coalescence around the actual hole was found. Thus it can be said that the cavity growth behavior obtained experimentally may reflect the real picture. The change in the k coefficient with material and testing condition may be explained by the approach presented by McClintock [25]. McClintock [25] examined the plastic deformation of circular defects in certain alloys and plasticine. By employing the effect of strain hardening during plastic deformation using the following expression:

$$\sigma = K\varepsilon^n \tag{6}$$

where n is the strain hardening exponent and K is a material parameter, it was found that the growth of cavities could be expressed theoretically by:

$$\ln = \frac{r}{r^0} = \frac{\bar{\varepsilon}\sqrt{3}}{2(1-n)} \sinh\left(\frac{\sqrt{3}(1-n)}{2}\frac{(\sigma_a + \sigma_b)}{\bar{\sigma}} + \frac{(\varepsilon_a + \varepsilon_b)}{2}\right) \tag{7}$$

where σ_a and σ_b, ε_a and ε_b are the principal stress and strain, $\bar{\sigma}$ is the equivalent stress, r and r^0 are the final

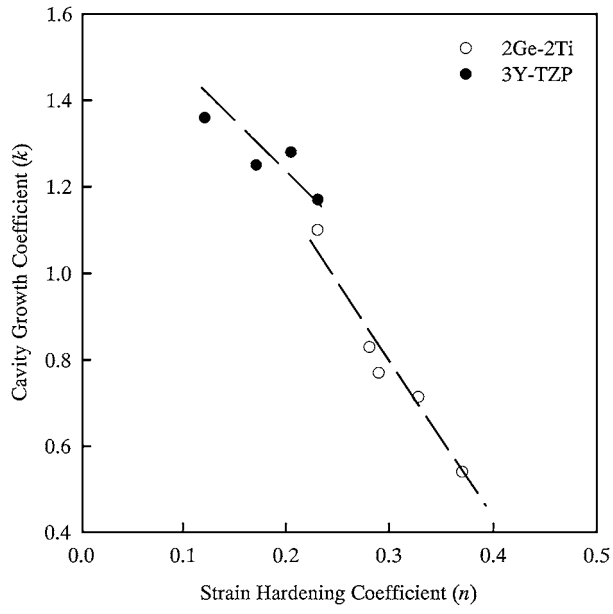

Figure 8 Change in cavity growth coefficient as a function of strain hardening.

and initial radii. The above expression indicates that hole growth is dependent on strain hardening and it was found to predict reasonably well the growth of holes under equi-biaxial tension, but tends to deviate under uniaxial conditions [25].

Such a relation between the strain hardening coefficient n and cavity growth coefficient k is presented in Fig. 8. Here the value of n was obtained from the stress-strain diagrams of these materials and fitted to Equation 6. It can be seen that there is a linear dependence between n and k, indicating that cavity growth can be inhibited by strain hardening.

Although a practical manner of examining the cavity growth in zirconia ceramics has been presented, there is a need for a theoretical treatment to distinguish between those effects attributed to superplastic "power law" phenomena and "strain hardening" need to be analyzed.

5. Conclusion

Cavity growth characterization was successfully carried out on 3Y-TZP and 2Ge-2Ti doped Y-TZP using pre-holed tensile specimens.

1. Tensile specimens with effective hole sizes of 450 μm were successfully produced using graphite fibers.

2. Micrographs of the failed pre-holded tensile specimens revealed that stress concentration around the circular defect in 3Y-TZP was significant, whereas in 2Ge-2Ti it was quite negligible.

3. Although the size of the defect introduced is relatively large compared to the grain size the deformation obtained was sufficient for qualitative and quantitative analysis of Y-TZP.

4. The % increase in cavity area was similar to the values obtained for 3Y-TZP for microscopic cavity growth.

5. It is proposed that for 3Y-TZP and 2Ge-2Ti, the cavity growth coefficients vary with strain rate and temperature, unlike metals, as a possible consequence of grain growth induced strain hardening.

References

1. J. W. HANCOCK, *Met. Sci.* **10** (1976) 319.
2. W. BEERE and M. V. SPEIGHT, *ibid.* **9** (1975) 190.
3. *Idem.*, *ibid.* **4** (1978) 172.
4. M. J. STOWELL, *ibid.* **9** (1980) 270.
5. A. C. F. COCKS and M. F. ASHBY, *ibid.* **8** (1980) 395.
6. D. W. LIVESEY and N. RIDLEY, *Met. Trans.* A **13A**(9) (1982) 1619.
7. J. BELZUNCE and M. SUERY, *Acta. Metall.* **31**(10) (1983) 1497.
8. P. A. FRIEDMAN and A. K. GHOSH, *Met. and Mat. Trans.* **17A**(12) (1996) 3827.
9. M. ZAKI, *ibid.* **27A**(4) (1996) 1043.
10. K. KANNAN and C. H. HAMILTON, *Scripta Mat.* **38**(2) (1998) 299.
11. J. R. PORTER, W. BLUMENTHAL and A. G. EVANS, *Acta Met.* **29** (1981) 1899.
12. R. L. TSAI and R. RAJ, *ibid.* **30** (1982) 1043.
13. D. J. SCHISSLER, A. H. CHOKSHI, T. G. NIEH and J. WADSWORTH, *Acta Metal. Mater.* **39**(12) (1991) 3227.
14. Z. C. WANG, N. RIDLEY, T. J. DAVIES and A. A. OGWU, *Acta Mat.* **44**(11) (1996) 4301.
15. Z. C. WANG, N. RIDLEY and T. J. DAVIES, *Scripta Mat.* **36**(5) (1997) 579.
16. *Idem.*, *J. Mater. Sci.* **34** (1999) 2695.
17. K. HIRAGA and K. NAKANO, *Mat. Sci. Forum* **243–245** (1997) 387.
18. K. HIRAGA, K. NAKANO, T. S. SUZUKI and Y. SAKKA, *Scripta Mat.* **39**(9) (1998) 1273.
19. *Idem.*, *Mat. Sci. Forum* **304–306** (1999) 431.
20. R. A. TAIT and D. M. R. TAIPLIN, *Scripta Met.* **13** (1979) 77.
21. D. S. WILKINSON and C. H. CACERES, *Mat. Sci and Tech.* **2** (1986) 1086.
22. H. CHOKSHI and T. G. LANGDON, *Met. and Mat. Trans.* A **27A** (1996) 2532.
23. K. SASAKI, M. NAKANO, J. MIMURADA, Y. IKUHARA and T. SAKUMA, *J. Am. Cer. Soc.* **84**(12) (2001) 2981.
24. G. E. DIETER, "Mechanical Metallurgy" (McGraw-Hill, New York, 1988).
25. F. A. MCCLINTOCK, *J. App. Mech.* **6** (1968) 363.

Received 10 April 2001
and accepted 25 February 2002